NJC

Accepted Manuscript

This is an *Accepted Manuscript*, which has been through the Royal Society of Chemistry peer review process and has been accepted for publication.

Accepted Manuscripts are published online shortly after acceptance, before technical editing, formatting and proof reading. Using this free service, authors can make their results available to the community, in citable form, before we publish the edited article. We will replace this *Accepted Manuscript* with the edited and formatted *Advance Article* as soon as it is available.

You can find more information about *Accepted Manuscripts* in the Information for Authors.

Please note that technical editing may introduce minor changes to the text and/or graphics, which may alter content. The journal's standard Terms & Conditions and the Ethical guidelines still apply. In no event shall the Royal Society of Chemistry be held responsible for any errors or omissions in this *Accepted Manuscript* or any consequences arising from the use of any information it contains.

ROYAL SOCIETY OF CHEMISTRY

www.rsc.org/njc

Experimental and Theoretical Studies of the ancillary ligand (*E*)-2-((3-amino-pyridin-4-ylimino)-methyl)-4,6-diterbutylphenol in Rhenium(I) core

Alexander Carreño[1,10*], Manuel Gacitua[2], Eduardo Schott[3], Ximena Zarate[4], Juan Manuel Manriquez[3], Marcelo Preite[5], Sonia Ladeira[6], Annie Castel[6], Nancy Pizarro[7], Andrés Vega[7,8], Ivonne Chavez[9], Ramiro Arratia-Perez[1,10]

[1]Doctorado en Fisicoquímica Molecular, Center of Applied Nanosciences (CENAP), Universidad Andres Bello, Ave. Republica 275, Santiago, Chile, Zip Code: 8370146.

[2]Departamento de Química Inorgánica, Facultad de Química, Pontificia Universidad Católica de Chile. Current addres: Center of Applied Ecology and Sustainability (CAPES), Universidad Adolfo Ibáñez, Peñalolén, Chile

[3]Laboratorio de Bionanotecnología, Universidad Bernardo O´Higgins, General Gana 1702, Santiago, Chile.

[4]Dirección de Postgrado e Investigación, Universidad Autónoma de Chile, Av. Pedro de Valdivia 641, Santiago, Chile.

[5]Departamento de Química Orgánica, Facultad de Química, Pontificia Universidad Católica de Chile.

[6]Université Paul Sabatier, Institut de Chimie de Toulouse (FR 2599), 118 route de Narbonne, 31062 Toulouse cedex 9, France.

[7]Departamento de Ciencias Químicas, Facultad de Ciencias Exactas, Universidad Andres Bello.

[8]Centro para el Desarrollo de la Nanociencia y la Nanotecnología, CEDENNA

[9] Departamento de Química Inorgánica, Facultad de Química, Pontificia Universidad Católica de Chile.

[10]Núcleo Milenio de Ingeniería Molecular para Catálisis y Biosensores, ICM

Abstract

The *fac*-[Re(CO)$_3$(**deeb**)**L**]$^+$ complex (**C2**) where **L** is (*E*)-2-((3-amino-pyridin-4-ylimino)-methyl)-4,6-diterbutylphenol ancillary ligand, which presents an intramolecular hydrogen bond, has been synthesized and characterized using UV-vis, ^{1}H-NMR, FT-IR, cyclic voltammetry and DFT calculations. The UV-vis absorption and emission properties have been studied at room temperature and the results were compared with TDDFT calculations including spin-orbit effects. We report an alternative synthesis route for the *fac*-Re(CO)$_3$(**deeb**)Br (**C1)** complex where **deeb**=(4,4'-diethanoate)-2,2'-bpy. Besides, we have found that the **C1** shows a red shift in the emission spectrum due to the nature of the ancillary electron donating ligand, while the **C2** complex shows a blue shift in the emission spectrum suggesting that the ancillary ligand **L** has electron withdrawing ability and the important role of the intramolecular hydrogen bond. The calculations suggest that an experimental mixed absorption band at 361 nm could be assigned to MLCT and LLCT transitions. The electron withdrawing nature of the ancillary ligand in **C2** explain the electrochemical behavior, which shows the oxidation of Re^I at 1.83 V and the reduction of **deeb** at -0.77 V.

Keywords

Rhenium (I) complexes, intramolecular hydrogen bond, electron withdrawing effect.

1. Introduction

The research of rhenium(I) tricarbonyl diimine complexes of the general form *fac*- $Re(CO)_3$(**N,N**)(**L**), where, **N,N** are substituted bipyridine and **L** the ancillary ligand might be halogen or pyridine, dates back from the 1970s. [1-2] Since then, it has attracted much attention due to their appealing photophysical properties, due to their luminescent properties based on the Re^I core which are adjustable, and might be optimized by the variation of the (**N,N**) ligand structure, or more subtly, by tuning the electronic nature of the ancillary ligand **L**. [3-5] Several conjugated chelating ligands, such as, diimine, indole and benzimidazoles, have been attached to the *fac*-$Re(CO)_3^+$ core showing therapeutic properties.[6]

On the other hand, Schiff bases having an -OH group at the ortho- position relative to an imino group -C=N- have generated much interest, due to the existence of an intramolecular hydrogen bond between the -OH and the nitrogen atom.[7-8] In addition, Gust *et. al.* [9] reported a benzimidazole substituent on bioinspired compounds that present an intramolecular hydrogen bond as dyes in sensitized solar cells. Furthermore, rhenium tricarbonyl complexes containing Schiff base ligands have been extensively studied as they display interesting photophysical properties. [10] Several studies about biological systems reported in literature have shown that the role of an intramolecular hydrogen bond in aminoacids like histidine is involved in the electron transport chain by the formation of phenoxy radicals. This fact has inspired the design of phenol benzimidazole molecules that have this kind of bond, which could be employed in catalysis. [11]

It is worthy to mention that there are several reports on Re^I complexes with ligands of different structure as dyes in light harvesting devices like the dye sensitized solar cells (DSSC), but their use is restricted because they only absorb in the yellow region of the spectra. [12] Hence, in this sense it would be possible to modulate the absorption energy introducing electron-donating or electron-withdrawing motifs, which would be able to modify the HOMO-LUMO energy gaps of the systems.
Besides, for a dye it is important to display properties like high molar extinction coefficients, low cost of production, diversity and directionality of the lowest energy excitation which has shown to be very important for the electron transfer process at the dye-TiO_2 interface, among others. [13]

Based on these facts, we focused on the study of a monodentate Schiff base, (*E*)-2-{[(3-aminopyridin-3-yl) imino]-methyl}-4,6-di-tert-butyl-phenol represented as the ancillary ligand **L** of the *fac*-$Re(CO)_3^+$ core. Interestingly, this ancillary **L** ligand shows an intramolecular hydrogen bond. (Scheme 1)

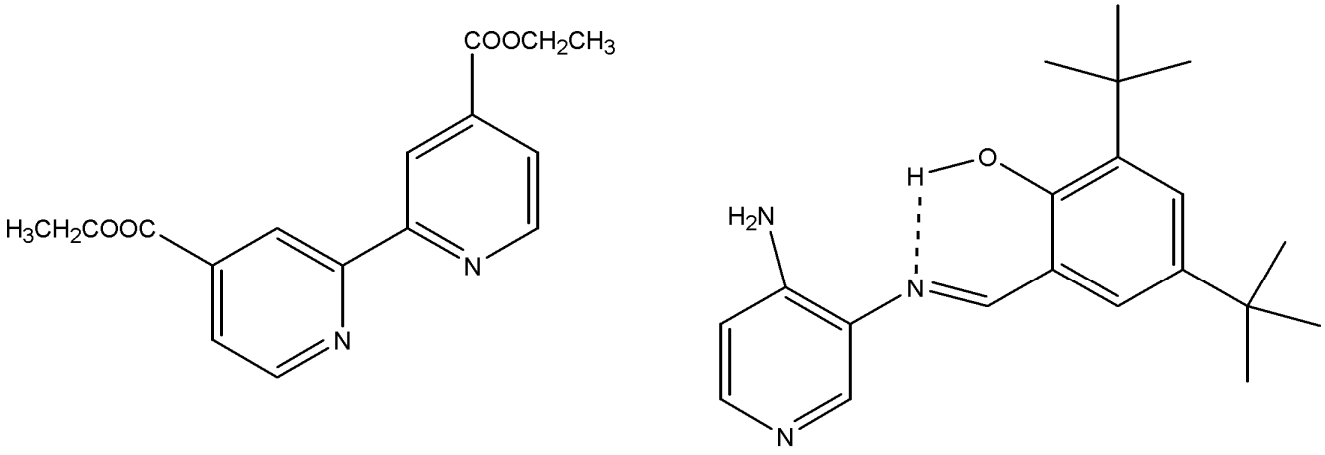

deeb **L**

Scheme 1. Structures of **deeb** and **L** ligands used in this work.

We report here an alternative synthesis of the *fac*-$Re(CO)_3$(**deeb**)Br (**C1)** complex with **deeb**=(4,4'-diethanoate)-2,2'-bpy and a new *fac*-$[Re(CO)_3$(**deeb**)(**L**)$]^+PF_6^-$ (**C2**) complex, where **C2** was characterized by means of FT-IR, ^{1}H-NMR, mass spectrometry, UV-Vis and emission spectra. Also, DFT and TDDFT calculations were performed in both complexes, including scalar and Spin-orbit (SO) relativistic effects since Rhenium is a quite heavy atom.

2. Experimental Section

2.1 Synthesis. All starting materials were purchased from Merck and Aldrich and used without further purification. The methods for preparation of the ancillary **L** ligand and the Re^I complex **(C2)** are given below:

The ancillary ligand (*E*)-2-((3-amino-pyridin-4-ylimino)-methyl)-4,6-diterbutylphenol, (L). A mixture of 3,4-diaminopyridine (9.16×10^{-3} mol) and 3,5-diterbutyl-2-phenylbenzaldehyde (9.16×10^{-3} mol) were added to a round bottom flask, and dissolved with 25 mL of ethanol at room temperature.[14] The mixture was stirred for 24 hours, concentrated to a 60% of the original volume and filtered. The crude product was washed with ethanol, and with diethyl ether. The resulting yellow solid (Yield 70 %) was dried under high vacuum. ^{1}H NMR (400 MHz, CD_3CN): δ= 1.32 [s, 9H, $C(CH_3)_3$], 1.46 [s, 9H, $C(CH_3)_3$], 4.98 [s, 2H, NH_2], 6.68 [d; J= 5.4 Hz; 1H], 7.42 [d; J=2.1 Hz; 1H], 7.51 [d; J=1.9 Hz; 1H], 8.02 [d; J=5.5 Hz; 1H], 8.04 [s, 1H], 8.74 [s, 1H], 13.26 [s, 1H]. UV/VIS: (acetonitrile, room temperature, c=4 x10^{-6} mol L^{-1}) λ(ε)= 221 (25637 mol^{-1} dm^3 cm^{-1}), 237(21388 mol^{-1} dm^3 cm^{-1}), 277(13145 mol^{-1} dm^3 cm^{-1}), 357(10022 mol^{-1} dm^3 cm^{-1}). FTIR (cm^{-1}): 3639 (νOH); 3481 (ν NH2);1612 (νCN).

Alternative synthesis of the *fac*-[Re(CO)$_3$(deeb)Br], (C1) complex. This complex was synthetized using an alternative and new route to the one published about a decade ago by Hasselman and Meyer [15]. The $(Re(CO)_3Br(THF))_2$ dimer, (5.92×10^{-4} mol) and 4,4'-$(COOCH_2CH_3)_2$-2,2'-bipiridyne (1.18×10^{-3} mol) were added to toluene (25 mL) and stirred for 20 min at room temperature. [16] The orange precipitate was collected, and recrystallized from ethanol. Orange crystals suitable for X-Ray diffraction were obtained by slow evaporation of the solvent. Yield 80 %. ^{1}H NMR (400 MHz, CD_3CN): δ= 1.44 [s, 6H, $(-CH_3)$], 4.49 [m, 4H, $-CH_2-$], 8,07[d, J=5.7 Hz; 2H], 8,96 [s, 2H], 9.20 [d, J=5.6 Hz; 2H]. UV-vis: (acetonitrile, room temperature, c= 5 x 10^{-5} mol L^{-1}) λ(ε)= 312 (16089 mol^{-1} dm^3 cm^{-1}), 419 (4201 mol^{-1} dm^3 cm^{-1}). FTIR (cm^{-1}) 2029 ; 1920 ; 1901 (νCO) ; 1730 (ν $COOCH_2CH_3$).

Synthesis of the *fac*-[Re(CO)$_3$(deeb)(L)](PF$_6$), (C2). To a suspension of **C1** (6.15×10^{-4} mol) in 40 ml of anhydrous THF and Ag(OTf) ($6,15\times10^{-4}$ mol) were added under an inert atmosphere in the dark, and left with stirring at room temperature for 2-3 hours. The precipitated AgBr biproduct was removed by filtration, and then the (*E*)-2((3-amino-pyridin-4-ylimino)-methyl)-4,6-diterbutylphenol (**L**) ($6,15\times10^{-1}$ mol) was then dissolved in anhydrous THF (30 mL) and added to the previous solution and refluxed for 5 h under a nitrogen atmosphere.[17] The solution was concentrated on a rotary evaporator, and the solid residue dissolved in ethanol. Excess NH_4PF_6 was added, and the mixture was stirred for 12 hours.

An orange solid of **C2** precipitated and collected, and recrystallized from ethanol/diethyl ether (1:1, V/V) with a 70% Yield.

^{1}H NMR (400 MHz, CD_3CN): δ= 1.35 [s, 9H], 1.42 [s, 9H], 1.44 [s, 6H, (-CH_3)], 4.49 [m, 4H], 5,92 [s, 2H, -NH_2], 6.45 [d; J=5.5 Hz; 1H], 7.28 [d; J=1.5 Hz; 1H], 7.47 [s, 1H], 7.51 [s, 1H], 7.53 [s, 1H], 8.11 [s, 1H], 8.20 [d; J= 5.5 Hz; 2H], 8.91 [s, 2H], 9.40 [d; J=5.6 Hz; 2H], 12,54 [s, -OH]. UV/VIS: (acetonitrile, room temperature, c= 2,17 x 10^{-5} mol L^{-1}) λ(ε)= 275 (23864 mol^{-1} dm^3 cm^{-1}), 361 (6789 mol^{-1} dm^3 cm^{-1}). FTIR (cm^{-1}): 3407 (νOH); 2871 (νNH_2); 2032 and 1923 (νCO) , 1733 (ν $COOCH_2CH_3$) , 1633 (νCN); 845 (νPF6-). M+/z: 895).

2.2 Characterization

UV-Vis and flourescence spectra were performed using a UV-Vis-NIR scanning spectrophotometer Shimadzu Model UV-3101 PC, and Perkin Elmer LS55 Luminescence Spectrometer. The NMR spectra were recorded on a Bruker AVANCE 400 spectrometer at 25 ºC. Samples were dissolved in deuterated acetonitrile, using tetramethylsilane as an internal reference. For the electrochemical experiments, the working solution contained 9.81×10^{-3} mol·L^{-1} of **L**, **deeb**, **C1** and **C2**, with 0.1 mol·L^{-1} of tetrabutylammonium hexafluorophosphate ($TBAPF_6$, in CH_3CN) as supporting electrolyte. Prior to each experiment the solution was purged with high purity argon, and an argon atmosphere was maintained over the solution during the whole experiment. A polycrystalline non-annealed platinum disc (diameter 2 mm) was used as working electrode. We used as counter electrode a platinum gauze of large geometrical area, separated from the cell main compartment by a fine grain sintered glass. All potentials quoted in this text refer to an Ag/AgCl electrode in tetramethylammonium chloride to match the potential of a saturated calomel electrode (SCE) at room temperature. All electrochemical experiments were performed at room temperature on a CHI900B bipotentiostat interfaced to a PC running the CHI 9.12 software that allowed experimental control and data acquisition.

2.3. Structure determination

A crystal of **C1** suitable for X-ray diffraction was obtained by slow evaporation of an ethanol solution at room temperature, yielding orange blocks. This crystal was introduced into a sealed capillary tube containing mother liquor. The intensity data collection was made on a Bruker Smart Apex diffractometer, using separation of 0.3° between frames and 10s by frame at 193 K. Triclinic system, P-1; a = 6.4256(2) Å, b =12.2609(4) Å, c = 13.0947(5) Å, α = 94.561(2)°, β = 101.729(2)° and γ =

94.970(2)°, $C_{39}H_{43}N_4O_8BrRe$, MM = 650.45.

The structure was solved by direct methods, using XS in SHELXTL and completed (non-H atoms) by Fourier difference synthesis.[18] During the final stages of the refinement of **C1** some disorder on the bromide and its trans carbonyl group was noticed. It suggests that two ligands, the bromide, and one carbonyl, may occupy randomly two trans-positions within the octahedral structure. The disorder was modelled considering two possible disordered positions, A and B, for the bromide and the carbonyl groups, with partial occupations adding up to **C1**. These were refined and held constant at 0.44 and 0.56 for A and B respectively, during the final cycles of refinement. Table 1 shows some experimental and refinement details.

Table 1. Crystal data and refinement details for **C1**.

FW/uma	650.45
Crystal System	triclinic
Space Group	P -1
a (Å)	6.4256(2)
b (Å)	12.2609(4)
c (Å)	13.0947(5)
α(°)	94.561(2)
β(°)	101.729(2)
γ(°)	94.970(2)
V (Å^3)	1001.31(6)
Z	2
d (g cm^{-3})	1.923
μ(mm^{-1})	8.108
F000	620
θrange	1.60 to 30.68.
hkl range	$-8 \le h \le 9$
	$-17 \le \kappa \le 17$
	$-17 \le \lambda \le 18$
N_{tot}, N_{uniq}	12977, 3740
(R_{int}), N_{obs}	(0.024), 3415

Refinement Parameters	302
GOF	1.196
R1, wR2 (obs)	0.0326, 0.0786
R1, wR2 (all)	0.0347, 0.0795
Max. and min Δρ	1.092 and -2.099

2.4. Computational methods

All the calculations reported here were carried out in the framework of the density functional theory (DFT) using the Amsterdam Density Functional computational package (ADF2012) via the Zeroth order regular approximation (ZORA) Hamiltonian including spin-orbit (SO) relativistic corrections and employing Slater Type Orbitals (STO) basis sets with triple-ζ accuracy plus one polarization function (TZP) for all the atoms.[19] The molecular geometry of the ground states and the oxidized and reduced states were fully optimized employing the BP86 functional.[20] In all cases, frequency analysis were performed after each geometry optimization, where we obtained non-imaginary frequencies verifying the local minima. The excitation energies were computed by time-dependent perturbation DFT (TDDFT) based on the linear response formalism within the iterative Davison procedure as implemented in the ADF code, employing the asymptotically correct van Leeuwen-Baerends (LB94) potential.[21] The calculations performed by first-principles method let us to obtain accurate excitation energies and oscillator strengths for the calculated complexes. Solvation effects were simulated by the Conductor-like screening model (COSMO) using acetonitrile as solvent, since this solvent was used in the UV-vis and cyclic voltammetry measurements.

4. Results and Discussion

The structures of **L**, **C1** and **C2** complexes are shown in Scheme 2. Complex **C1** was previously published by Hasselmann and Meyer [15] obtained by a traditional route to afford rhenium tricarbonyl diimine. This procedure involved the reaction of a **deeb** with bromo rheniumpentacarbonyl at reflux under constant nitrogen atmosphere by 3-4 h, obtaining tricarbonyl bromodiimine rhenium species. In this work, **C1** was prepared by a different route by reacting bromotricarbonyl(tetrahydrofuran)rhenium

(I) dimer with 4,4'-(ethanoate))$_2$-2,2'-bipyridine (**deeb**) in a ratio 1:2 in toluene at room temperature for 20 min, which is similar to a method reported by Venegas *et al.*[16] The synthesis of (*E*)-2-((3-amino-pyridin-4- ylimino)-methyl)-4,6-diterbutylphenol **L** was previously reported by Kleij *et. al*. [14].

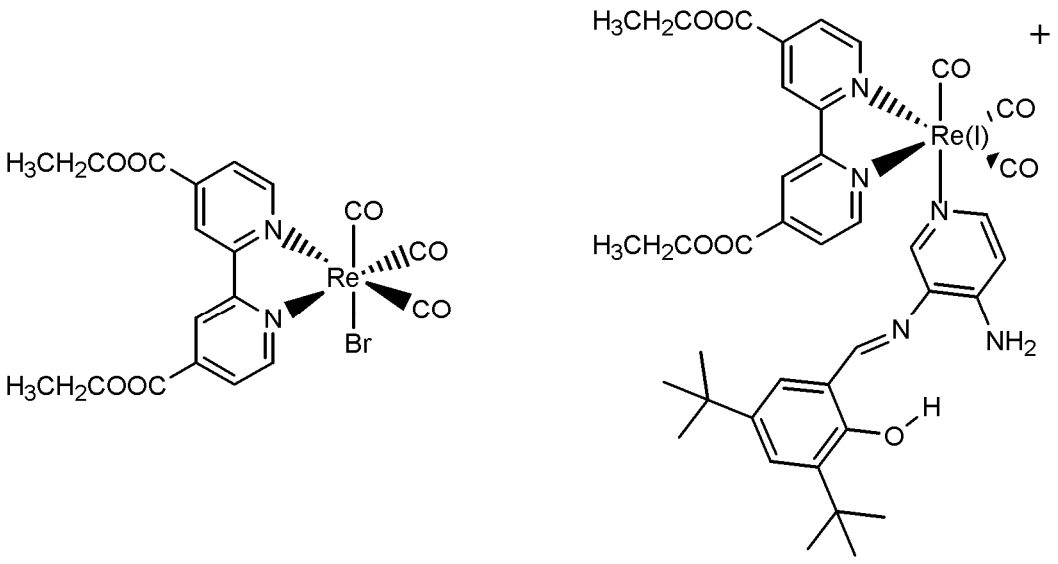

C1 **C2**

Scheme 2. Structure of **C1** and **C2** complexes.

The presence of the carbonyl groups in complexes **C1** and **C2** was observed by FTIR experiments, which show the characteristic three infra-red active modes [A'(l) + A'(2) + A"], observed at 2029, 1920 and 1901 cm^{-1} for **C1**, and at 2032 and 1923 cm^{-1} for **C2**, which are assigned to a facial (fac) isomer arrangement.[22] In case of **C2** only two bands were observed due to the local symmetry loss. The complexes **C1** and **C2** present a fac isomer arrangement because a characteristic property of mer-isomers arrangement of $Re(CO)_3$ is the very low IR intensity of the highest frequency band with respect to the other two bands, which is not observed. On the other hand, the values for the CO vibrational bands in both complexes indicates that metal backbonding effects are acting since these values are smaller than free ν(CO) suggesting an Re-C bond lengthening and C-O bond shortening.[23] In addition, a stretching assigned to C=O in the ester groups in the **deeb** ligand was observed at 1730 cm^{-1} for **C1** and at 1733 cm^{-1} for **C2**. In the case of **C2**, a signal observed at 845 cm^{-1} is assigned to the PF_6^- anion. The C=N stretching in the free ligand **L** was located at 1612 cm^{-1} and 1633 cm^{-1} for **C2**.

We report here the crystal structure of **C1**, that shows a monometallic *fac*-Re(**deeb**)$(CO)_3$(Br) molecule having a *fac*- correlation of the three carbonyl ligands according to the observed FTIR. Coordination is

completed by the **deeb** ligand and bromide, see Figure 1. The observed Re-N2 bond distance is 2.176 Å which is well determined by the theoretically optimized geometry of 2.193 Å. The Re-C(CO) (Re-C2, 1.936(5) Å; Re-C3, 1.937(9) Å and C-O (C2-O2, 1.142(6) Å) bond distances are found as expected for similar rhenium carbonyl complexes.[24] Selected bond lengths and bond angles are shown in Table 2. The geometry of **C1** was optimized in its singlet state by the DFT method with the BP86 functional. All other calculated bond lengths are well correlated with the X-ray crystal structure data.

Table 2. Selected bond distances (Å) and angles (º) for **C1**. Calculated values are provided for comparison.

	Calc.	**Exp.**
	d (Å)	
Re-Br	2.709	2.564(11)
Re-C3	1.921	1.937(9)
Re-C2	1.937	1.936(5)
Re-N2	2.193	2.176(3)
	ang (˚)	
C3-Re-N1	93	95(3)
C3-Re-C2	90	88(3)
Br1-Re-C3	179	175(3)
N1-Re-C2	172	172(17)

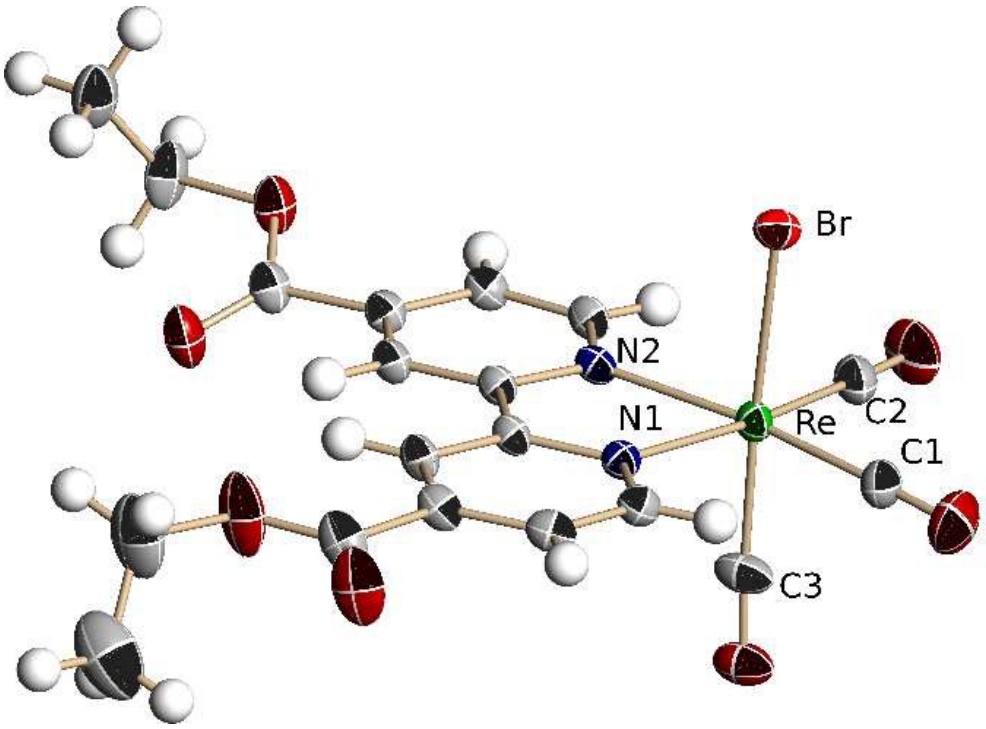

Figure 1. Molecular structure diagram for **C1** showing partial atom numbering. Displacement ellipsoids drawn at the 50% level of probability.

The ^{1}H-NMR spectrum for **L** shows a singlet at 13.26 ppm, which was assigned to the intramolecular hydrogen bond (see Figure S1 in the Supplementary Information), while the amino proton was assigned to a singlet located at 4.98 ppm, as previously reported for similar compounds.[25] After addition of D_2O, both signals disappear from the spectrum, which corroborate our assignment (data not shown). The signals of the *tert*-butyl group appear at 1.46 and 1.32 ppm, and the aromatic protons of both rings appear at 6.68 (d, 5.4 Hz); 7.42 (d, 2.1 Hz); 7.51 (d, 1.9 Hz); 8.02 (d, 5.5 Hz); 8.04 (s) and 8.74 (s) ppm.

The equivalence of the proton peak signals in the ^{1}H-NMR spectra revealed the symmetrical nature of the **deeb** ligand in both **C1** and **C2** complexes. [26] 1D and 2D NMR spectra were obtained in deutered acetonitrile for **C2**. After formation of the **C2**, the ^{1}H-NMR shows relevant changes in the chemical shift relative to the **deeb** and **L** ligands. The aromatic proton resonances from the **deeb** ligand appear at 8.07 (dd, 5.7 Hz); 8.96 (s) and 9.20 (d, 5.6 Hz) ppm in **C1** (see Figure S2) according to those reported by Hasselman *et al* [15]. For **C2** the corresponding values are 8.20 (dd, 5.5 Hz); 8.91 (s) and 9.40 (d, 5.6 Hz) ppm (see Figures S3 and S4). Note the downfield shifting of the chemical shifts, when

compared to **C1**. In contrast, the signals attributed to the ancillary ligand **L** shift to higher field, appearing at 6.45 (d, 5.5 Hz); 7.28 (d, 1.5 Hz); 7.47 (s); 7,51 (s); 7.53 (s); 8.11(s) ppm for the aromatic signals, and at 12.5 ppm for the -OH group. The ESI mass spectrum of **C2** (see Figure S5) shows a major fragment at m/z = 895 which is in agreement with the expected value for the molecular ion.

The absorption spectra of **C1** and **C2** in CH_3CN were recorded at room temperature. It can be observed that the spectrum of **C1** is dominated by an intense absorption band centered at 312 nm (ε=1.61x10^4 dm^3 mol^{-1} cm^{-1}) and at λ_{max}= 419 nm (ε=4.20x10^3 dm^3 mol^{-1} cm^{-1}), according to Hasselman *et al*. These transition are typically found for analogous complexes.[27] In the case of **C2**, two blue-shifted absorption bands can be appreciated at λ_{max}= 275 nm (ε=2.38x10^4 dm^3 mol^{-1}cm^{-1}) and at λ_{max}= 361 nm (ε=6.78x10^3 dm^3 mol^{-1} cm^{-1}). The first one corresponds to the $\pi\rightarrow\pi^*$ intraligand (IL) transition, while the second one is usually assigned to a metal-to-ligand charge transfer (MLCT) transition by analogy with similar compounds. [28] It can also be associated with an interligand charge transfer transition (LLCT) from a ligand **L** to an **deeb** ligand, as it is discussed by the theoretical studies below.
Figure 2 shows the room-temperature UV-vis absorption and emission spectra for **C1** and **C2** in dichloromethane. **C1** shows a broad emission band, with a maximum at 660 nm, when the complex is excited at 375 nm or 435 nm (which are the wavelengths of absorption). This broad emission bands is characteristic for MLCT transitions.[29] A large Stokes shift can be observed, which evidence a large change in the dipole moment between the ground and excited states. This emission process is characteristic for rhenium(I) tricarbonyl complexes.[30] Moreover, the greater the electron-donor effect of the bromide ligand in **C1**, the emission gets more red-shifted.
Under the same conditions of excitation for **C2**, a less intense broad emission band shifted to a lower wavelength of 610 nm (see Figure 2). It has been suggested by photophysical data of analogous Re(I) complexes (with **L**= substituted pyridines) that a shift to shorter wavelength for the emission is due to the cationic nature of the complexes.[31] However, other studies on similar rhenium tricarbonyl complexes described the shift to lower wavelengths as due to different substituent groups over the ancillary ligands of these cationic complexes. These studies demonstrated the modulation effect over the rhenium complexes including bpy/X-py (where X is the substituent over pyridine). In this sense, the presence of $d\pi(Re)\rightarrow\pi^*$ or $\pi\rightarrow\pi^*$ transitions bands depends upon the electronic character of the ancillary ligand. [32-33] Thus, the blue shift observed in **C2** in both solvents could be attributed to the electron-withdrawing nature of the (E)-2-((3-amino-pyridin-4-ylimino)-methyl)-4,6-diterbutylphenol (**L**) ancillary ligand. For completeness, this effect is discussed with electrochemical data given below.

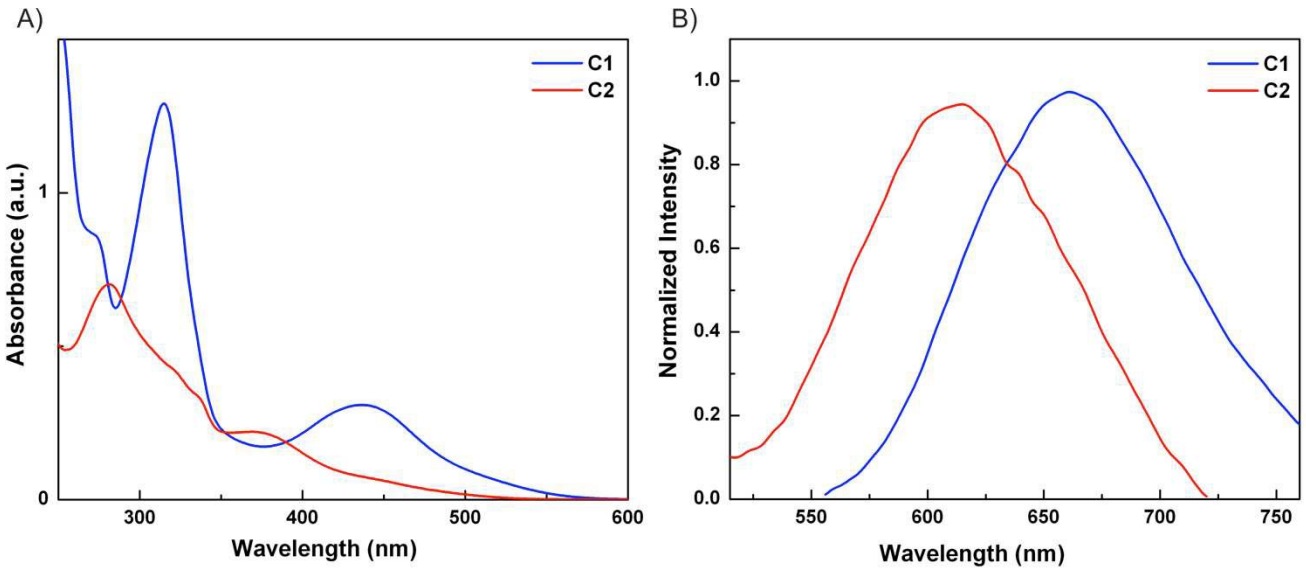

Figure 2. UV-vis absorption (A) and emission (B) spectra for **C1** (blue line) and **C2** (red line) in CH_2Cl_2.

The studies of cyclic voltammetry profiles showed several signals, which were solved by studying the working window potential. By comparing the stable profile of each compound, Figure 3, several characteristics can be noticed (from top to bottom).

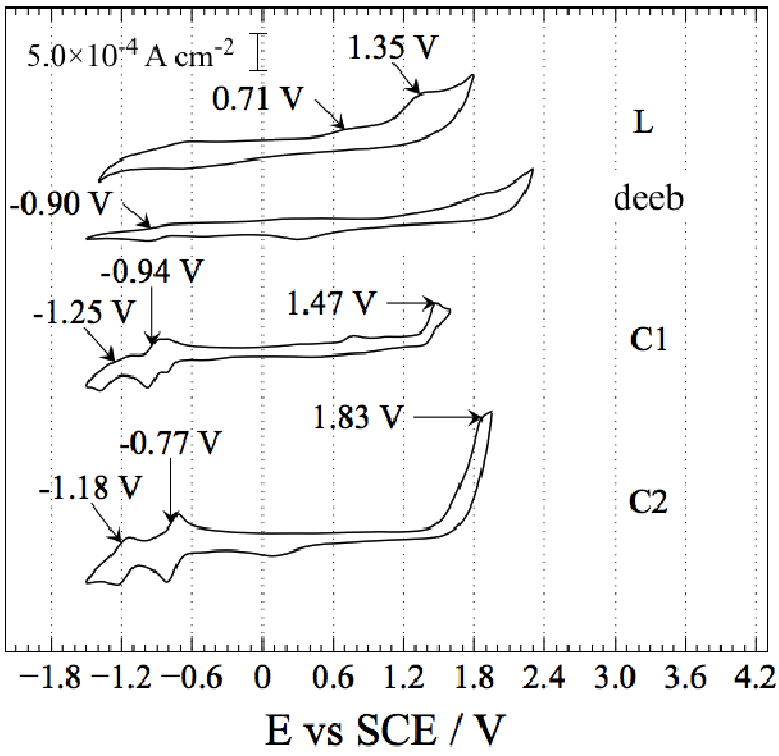

Figure 3. CV profiles comparison of ligands and complexes at 200 mVs^{1}. Interface: Pt | 1.0 x 10^{-5} M of analyte + 1.0 x 10^{-4} M $TBAPF_6$ in anhydrous CH_3CN under an argon atmosphere.

The ligand **L** presents only two important irreversible oxidant processes at peak potential, E_p, 0.71 V and 1.35 V. The **deeb** ligand has, in contrast, a reversible reduction process at a half-wave potential, $E_{½}$, of -0.90 V and is not worth-discussing the anodic process (Figure S6).

For understanding the electrochemical properties of **C1** and **C2**, electrochemical data of reagent $Re(CO)_5Br$ since model complex was studied (Figure S7). This compound presents two irreversible processes, an oxidation at E_p 2.04 V and a reduction at E_p -1.74 V. The oxidation is associated with a metal centre oxidation Re (I) → Re (II), and reduction from Re (I) → Re (0) respectively. [34-37]

In **C1**, rhenium oxidation appears at E_p 1.47 V according with the value reported by Hasselman et al. [15] Also, the reversible reduction of **deeb** is present at $E_{½}$ -0.94 V, which is more distinguishable at the working window study (Figure S8). Rhenium reduction appears at less energetic values, and

becomes, at first glance, a quasi-reversible process at $E_{½}$ -1.25 V. Such signal has been attributed to a Re (I) → Re (0) process.[38-40] Other authors, using bpy ligands, have reported the same reductions values with different degrees of reversibility, because the redox potentials for the rhenium complexes depend on the nature of the ligands. [41] Regardless if these reductions processes may be attributed specifically to a particular moiety, by the shape and position of the peaks it's seems that the electrochemical reaction follow a typical electrochemical-electrochemical-chemical reaction mechanism (EEC) previously described by Manbeck *et al.* [37] with bromide dissociation as the chemical step:

$$[Re(deeb)(CO)_3Br] + e \rightleftharpoons [Re(deeb)(CO)_3Br]^- \quad E_{½}: -0.94\ V\ (i)$$

$$[Re(deeb)(CO)_3Br]^- \rightarrow [Re(deeb)(CO)_3] + Br^- \quad , slow\ (ii)$$

$$[Re(deeb)(CO)_3Br]^- + e \rightleftharpoons [Re(deeb)(CO)_3Br]^{2-} \quad E_{½}: -1.25\ V\ (iii)$$

$$[Re(deeb)(CO)_3Br]^{2-} \rightarrow [Re(deeb)(CO)_3]^- + Br^- \quad , fast\ (iv)$$

The rhenium oxidation for **C2** takes place at a higher potential (1.83 V., all defined, Figure S9), and showed an irreversible process with only oxidative peak potential, according to analogous complexes.[42] Hence, the replacement of Br^- by **L** has a notorious influence on the oxidation value for Re (I) → Re (II). In this sense, this process occurs at higher potentials relative to the **C1**, which means that **L** has an electron-withdrawing effect over the positive charge on the rhenium atom. This produces a decrease in the electron density and makes it less easily oxidizable. On the other hand, there are two reversible reduction processes at -0.77 V and -1.18 V that could be assigned to the same processes seen in **C1**. This means that reduction processes require less energy to occur and, particularly, the Re (I) → Re (0) reduction becomes even more reversible. Such behavior is also explained by the fact that **C2** has no halide attached to its core; since no chemical dissociation step occurs during the mechanism, then, by preventing bromide (strong anionic character) liberation in anhydrous solvent, $E_{½}$ for reduction of **C2** decreases (requires less energy). Moreover, **deeb** reduction in **C2** takes places at a less negative potential compared to its precursor **C1**, hence **L** has an effect over **deeb**, too. The more pronounced electron-withdrawing character of **L** facilitates the reduction of **deeb**. Therefore, there is higher inter-ligand electron displacement from **deeb**, going through rhenium to **L**, which is in agreement with the blue shift observed in the UV-vis spectra. Also, this could explain the diminishing of the reduction potential and the higher reversible character of the Re (I)→ Re (0) process.[43-46].

Computational optimizations of the oxidized and reduced states of the studied compounds, **deeb**, **C1** and **C2**, were performed. The highest occupied molecular orbitals are reported in the supplementary

information (Figure S10) where it is possible to observe concordance with the experimental results. In **C1**, the highest occupied single molecular orbital is localized in the metal which indicate that the removed electron used to localize in this fragment. For the reduced state, the orbital shows that the gained electron is localized in the **deeb** motif. On the other hand, in case of **C2**, it can be seen that the oxidized state displays a contribution of the ligand which could be attributed to the electron withdrawing nature of the ligand. The reduced structure shows as well as **C1**, that the gained electron is localized in the **deeb** motif. Besides it is observed that the rings of the ligand in this optimized reduced structure suffer a rotation maintaining the hydrogen bond.

To go further in our understanding of the effect of the monodentate Schiff-base ancillary ligand **L** over the complex, DFT calculations, including SO relativistic effects, were carried on. As the SO effect is included, double groups irreducible representation (irreps) need to be used, where the high occupied molecular orbitals (HOMO) were transformed to the highest occupied molecular spinor (HOMS). [47-48]

The HOMS and HOMS-1 spinors for **C1** have the mixed contribution of dπ(Re), pπ(Br) and π^*-orbitals of CO. The LUMS and LUMS+1 have π* character correspond to π* orbital on **deeb**. In **C2** the HOMS is located mainly over the **L** ligand, mostly in the intramolecular hydrogen bond, and corresponds to the π orbital of **L**. HOMS-1 have the major contribution of dπ(Re). On the other hand, the LUMS is centered on the **deeb** ligand and LUMS+1 has π* character centred around of pyridine and phenol rings on the **L** ligand.

The isosurfaces of the HOMS and LUMS of both complexes are shown in Figure 4. Frontier molecular orbitals (MO) play a relevant role in such systems because they rule the electronic excitations and the nature of transition. The percentage compositions of the involved orbitals are reported in the supplementary information (Table S1 and Table S2).

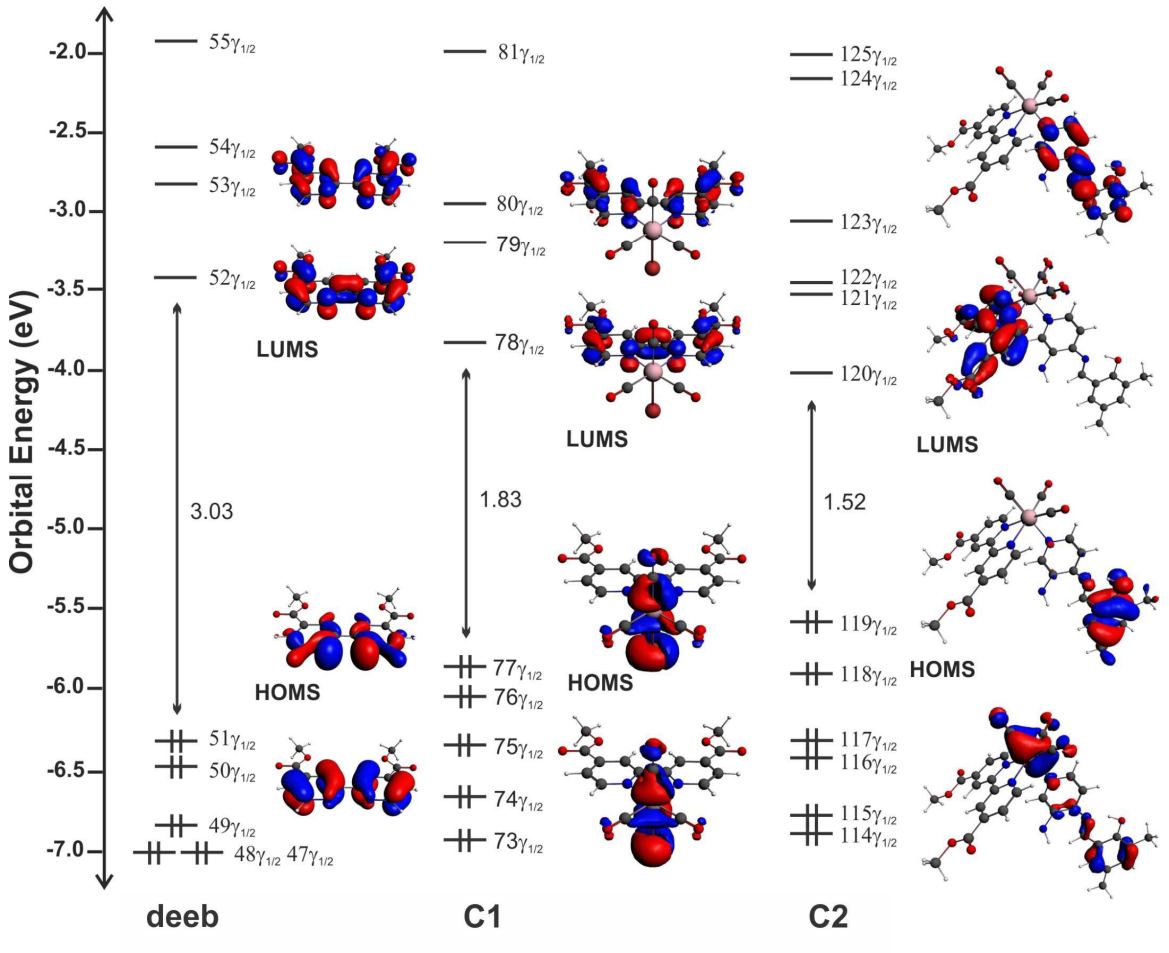

Figure 4. Energy levels diagram and isosurfaces plots of the MOs for compounds **deeb, C1** and **C2** as obtained from SO-BP86 calculations.

TDDFT calculations on the optimized geometry of **C1** and **C2** were performed in acetonitrile as solvent, see Table 3 for more details. The dominant excitation for **C1** at 273 nm (4.54 eV) is $64\gamma_{1/2} \rightarrow 78\gamma_{1/2}$ and has been assigned as intraligand charge transfer (ILCT) transition, while the bands at 391 nm (3.17 eV) is $75\gamma_{1/2} \rightarrow 80\gamma_{1/2}$ have dπ(Re) → deeb(π*) character being therefore MLCT (see Figure 5). Both calculated transitions show good agreement with the bands observed at 312 nm ($\varepsilon=1.61\times10^4$ $dm^3\ mol^{-1}\ cm^{-1}$) and at λ_{max}= 419 nm ($\varepsilon=4.20\times10^3$ $dm^3\ mol^{-1}\ cm^{-1}$) recorded in acetonitrile.

The calculated vertical electronic transitions for **C2** show two important transition at 365 nm (3.39 eV) and at 369 nm (3.36 eV) corresponding to $111\gamma_{1/2} \rightarrow 120\gamma_{1/2}$ and $114\gamma_{1/2} \rightarrow 123\gamma_{1/2}$. These transitions have a π(L) →π*(deeb) and dπ(Re)→π*(deeb) character, and are of type LLCT and MLCT. These two calculated transition are in good agreement with the experimental values. Figure 5 and 6 resume the principal excitations for **C1** and **C2**. Also is important to notice that **C1** (3.17 eV) showed an

electronic transition energy smaller than **C2** (3.39 eV) suggesting the electron withdrawing effect of **L**, what is consistent with the investigations of Sacksteder *et al* who verified the dependence of the acceptor/donor abilities of ancillary ligands in the properties of the rhenium core.[32]

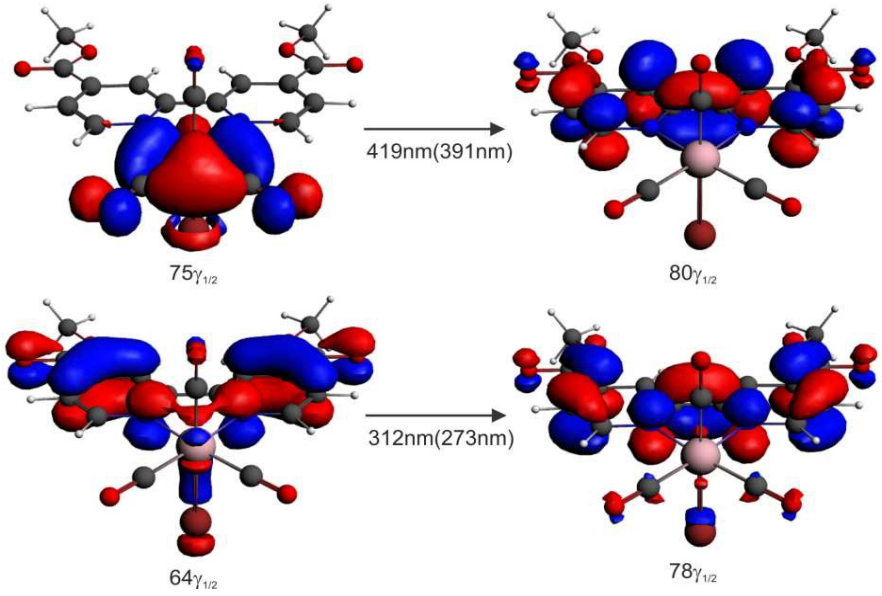

Figure 5. Active molecular orbitals isosurfaces of **C1**.

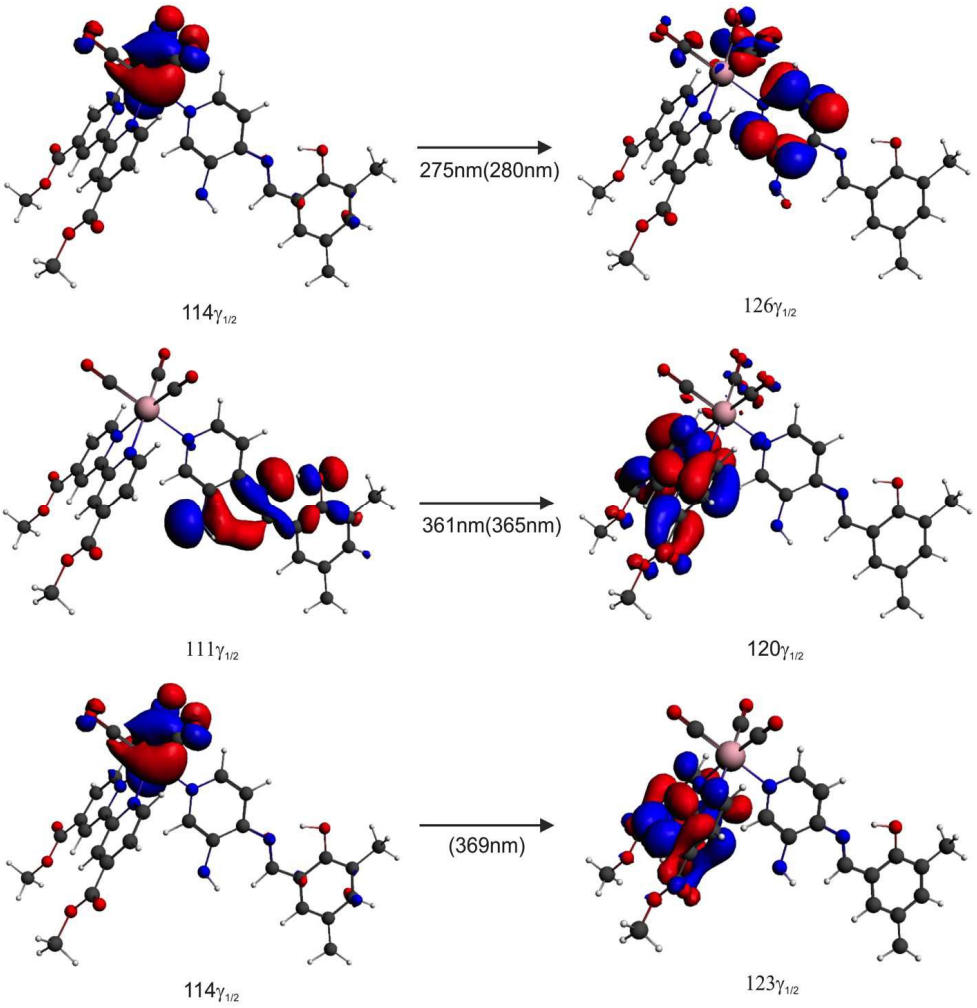

Figure 6. Active MOs isosurfaces of the calculated transitions for **C2**.

Table 3. Calculated (λ_{calc}) and experimental (λ_{exp}) wavelengths in nm. Energy (E) in eV, oscillator strength *f*, active MOs and their contributions in %, type of the electronic transitions for the vertical excitations from TD-DFT and character (C) of the calculated transitions.

	λ_{exp}	λ_{calc}	E	*f*	%Orbital Contribution				C
C1	312	273	4.54	0.111	$64\gamma_{1/2}$	->	$78\gamma_{1/2}$	42	ILCT
	419	391	3.17	0.002	$75\gamma_{1/2}$	->	$80\gamma_{1/2}$	82	MLCT
C2	275	280	4.43	0.001	$114\gamma_{1/2}$	->	$126\gamma_{1/2}$	32	ILCT
					$116\gamma_{1/2}$	->	$130\gamma_{1/2}$	15	MLCT
	361	365	3.4	0.156	$111\gamma_{1/2}$	->	$120\gamma_{1/2}$	52	LLCT
		369	3.36	2.00E-002	$114\gamma_{1/2}$	->	$123\gamma_{1/2}$	72	MLCT

On the other hands, **C1** and **C2** showed important differences in the electronic energy levels due to the change of the ancillary ligand. Bromide in **C1** has electron donating ability compared with **L** ligand in **C2,** which shows electron withdrawing ability. This change causes a narrow electronic transition energy gap [49-50], with values of 1.83 eV for **C1** and at 1.52 eV for **C2**. Furthermore, T. Liu et. al. [51-52] reported earlier that the LUMO energy is also affected by the nature of the ancillary ligand, showing in other complexes the stabilization in energy of the LUMO due to the introduction of an electron withdrawing ligand. On the other hand, the HOMO remains almost unaltered. In our case, LUMS energy is observed at -3.7 eV for **C1** and at -4.0 eV for **C2**. The stabilization observed for the LUMS in **C2** is due to the electron withdrawing ability of **L,** which has contribution from the stability of the intramolecular hydrogen bond, which is also consistent with all the experimental results. The strength of the hydrogen bond was calculated by forcing the non-containing hydrogen bond structure. It was found that the structure including the hydrogen bond is more stable by 0.49eV (11 Kcal/mol). The optimized structure of **C2** without the hydrogen bond is shown in Figure S11.

5. Conclusions

The rhenium carbonyl complex containing the *fac*-$Re(CO)_3^+$ core and the Schiff base ancillary ligand (**L**) which presents an intramolecular hydrogen bond with general formula *fac*-$Re(CO)_3$(**deeb**)**L** (**C2**) have been synthesized and characterized by both experimental and theoretical studies. It is worth to mention that the **C1** precursor complex used in the syntheses of **C2** was obtained by an alternative method, using as precursor a rhenium (I) dimer at room temperature, with high yield. The **C1** crystal

structure was determined by X-ray crystallography, showing a distorted octahedral coordination geometry. The exchange of bromide in **C1** complex by an ancillary ligands **L** in **C2** kept the facial (fac) isomer arrangement and not mer symmetry, as confirmed by the FT-IR study.

The electron-withdrawing effect of the **L** ligands in **C2** complex were observed by ^{1}H-NMR, absorption and electrochemical studies. The UV-vis absorption spectra of **C2** compared with the corresponding **C1** show a blue shift.

The electronic transitions computed by TDDFT method including SO relativistic effects show good agreement with the experimental data. The electronic studies showed that the absorption band is dominated by MLCT and LLCT transition at 361 nm ($111\gamma_{1/2} \rightarrow 120\ \gamma_{1/2}$ and $114\gamma_{1/2} \rightarrow 123\gamma_{1/2}$) for **C2** which involve orbitals located in the hydrogen bond.

The stability of the intramolecular hydrogen bond suggests the role of the electron withdrawing effect of **L** in **C2** and this was confirmed by theoretical calculations. Thus, the introduction of the electron-withdrawing ancillary ligand to the rhenium core narrows the HOMS-LUMS electronic energy gap, which means that the UV-vis absorption spectrum could be shifted toward the visible region and the LUMS orbital could get near in energy to the conduction band (-4.0 eV) of the semiconductor TiO_2. Besides that the lowest energy transition displays a charge separation since the involved orbitals are located in different fragments of the molecule.

Finally, a correlation between the electron withdrawing effect from the ligand **L** and the redox potential values was also observed. In **C1**, rhenium oxidation appears at 1.47 V and at 1.83 V for **C2**.

Supporting Information: CCDC 892694 contains the supplementary crystallographic data for **C1**. These data can be obtained free of charge from The Cambridge Crystallographic Data Centre via www.ccdc.cam.ac.uk/data_request/cif. Supplementary data associated with this article can be found, in the online version.

Acknowledgements

Funded by Project RC120001 of the Iniciativa Científica Milenio del Ministerio de Economía, Fomento y Turismo, ECOS-CONICYT C08E01, UNAB-DI-28-10/I project, FONDECYT 1120865, 1141138,

1150629, 1130707, 11140563 and 1114056. A.V. is member of the Financiamiento Basal para Centros Científicos y Tecnológicos de Excelencia FB0807. We are grateful to Dr. Maria A. Del Valle (UC) for instrumentals facilities and Dr. Barbara Loeb L. (UC) for valuable discussions. We thank B.A. Alfonso Inzunza G. for his help with the English translation. Dedicated to the loving memory of Dr. Ana Maria Leiva Maturana (RIP).

References

[1] M. Wrighton, D. Morse, J. Am. Chem. Soc., 101 (1979) 2888.

[2] A. El Nahhas , A. Cannizzo, F. van Mourik, A.M. Blanco-Rodriguez, S. Zalis, A. Vlcek, M. Chergui, J. Phys. Chem. A, 114 (2010) 6361.

[3] T.M. McLean, J.L. Moody, M.R. Waterland, S.G. Telfer, Inorg. Chem., 51 (2012) 446.

[4] L.A. Worl, R. Duesing, P. Chen, L. Della Ciana, T.J. Meyer, J. Chem. Soc. Dalton Trans. (1991) 849.

[5] K.K.W. Lo, M.W. Louie, K.Y. Zhang, Coord. Chem. Rev., 254 (2010) 2603.

[6] D.K. Orsa, G.K. Haynes, S.K. Pramanik, M.O. Iwunze, G.E. Greco, D.M. Ho, J.A. Krause, D.A. Hill, R. J. Williams, S.K. Mandal, Inorg. Chem. Comm., 11 (2008) 1054.

[7] M. Holbach, X. Zheng, C. Burd, C.W. Jones, M. Weck, J. Org. Chem. 71 (2006) 2903.

[8] A. Carreño, A. Vega, X. Zarate, E. Schott, M. Gacitua, N. Valenzuela, M. Preite, J.M. Manriquez, I. Chavez, Quim. Nova, *37* (2014) 584.

[9] D. Gust, T. A. Moore, A. L. Moore, Acc. Chem. Res., 42 (2009), 1890.

[10] M.S. Jana, A.K. Pramanik, S. Kundu, D. Sarkar, T.K. Mondal, Inorganica Chimica Acta, 399 (2013) 138.

[11] G.F. Moore, M. Hambourger, G. Kodis, W. Michl, D. Gust, T.A. Moore, A.L. Moore, J. Phys. Chem. B, 45 (2010), 14450.

[12] K.C. Gupta, A.K. Sutar, Coord. Chem. Rev. 252 (2008) 1420.

[13] J. Chua, N. Mathews, S.G. Mhaisalkar, S.J. Moon, S.M. Zakeeruddin, M. Grätzel., J.Phys.Chem.C., 117 (2013), 10980.

[14]A.W. Kleij, M. Kuil, D.M. Tooke, M. Lutz, A.L. Spek., J.N.H. Reek, Chem. Eur. J., 11 (2005) 4743.

[15] G.M. Hasselmann, G.T. Meyer, J. Phys. Chem. B, 103 (1999) 7671.

[16] F. Venegas, N. Pizarro, A. Vega, J. Chil. Chem. Soc., 56 (2011) 682.

[17] R.B. Lopez, B. Loeb, D. Striplin, M. Devenney, K. Omberg, T.J. Meyer, J. Chil. Chem. Soc., (2004) 49.

[18] SHELXL-PC Package. Bruker Analytical X-ray Systems, Madison, WI, 1988.

[19] X. Tu, E. Alster, A. Muñoz-Castro, R. Arratia-Perez, G.S. Nichol, Z. Zheng, Chem. Eur. J., 17 (2011) 580.

[20] K. Hu, H.A. Severin, B.D. Koivisto, K.C.D. Robson, E. Schott, R. Arratia-Perez, G.J. Meyer, C.P. Berlinguette, J. Phys. Chem. C., 118 (2014) 17079

[21] L.E. Roy, T. Hughbanks, Inorg. Chem., 45 (2006) 8273.

[22] A. Kumar, S. Sun, J.A. Lees, Organomet. Chem., 29 (2010) 1.

[23] G. Herzberg, Molecular Spectra and Molecular Structure, Second Edition (1950).

[24] B.J. Liddle, S.V. Lindeman, D.L. Reger, J.R. Gardinier, Inorg. Chem., 46 (2007) 8484.

[25] D.H. Waldeck, Chem. Rev. (1991) 415.

[26] L.N. Winslow, D. P. Rillema, J. H. Welch, P. Singh, Inorg. Chem., 28 (1989) 1596.

[27] R. Sahai, D.P. Rillema, R. Shaver, S. Van Wallendael, D.C. Jackman, Inorg. Chem, 28 (1988) 1022.

[28] R. Alberto, R. Schibli, R. Waibel, U. Abram, A.P. Schubiger, Coord. Chem. Rev., 190 (1999) 901.

[29] D.J. Stufkens, A. Vlcek, Coord. Chem. Rev, 177 (1998) 127.

[30] A.J. Amoroso, M.P. Coogan, J.E. Dunne, V. Fernandez-Moreira, J.B. Hess, A.J. Hayes, D. Lloyd, C. Millet, S.J.A. Pope, C. Williams, Chem. Commun., (2007) 3066.

[31] J.L. Smithback, J.B. Helms, E. Schutte, S.M. Woessner, B.P. Sullivan, Inorg. Chem., 45 (2006) 2163.

[32] L. Sacksteder, A.P. Zipp, E.A. Brown, J. Streich, J.N. Demas, B.A. DeGraff, Inorg. Chem., 29 (1990) 4335.

[33] A. Ito, Y. Kang, S. Saito, E. Sakuda, N. Kitamura, Inorg. Chem., 51 (2012) 7722.

[34] J.C. Luong, L. Nadjo, M.S. Wrighton, J. Am. Chem. Soc., 100 (1978) 5790.

[35] A. Juris, S. Campagna, I. Bidd, J.M. Lehn, R. Ziessel, Inorg. Chem, 27 (1988) 4007

[36] M.Bakir, Journal of Electroanalytical Chemistry 466 (1999) 60

[37] G. F. Manbeck, J. T. Muckerman, D. J. Szalda, Y. Himeda, E. Fujita, J. Phys. Chem. B, DOI:10.1021/jp511131x

[38] Q. Zeng, M. Messaoudani, A. Vlcek Jr., F. Hartl, Eur. J. Inorg. Chem., (2012) 471.

[39] L. Wallace, D.P. Rillema, Inorg. Chem., 32 (1993) 3836.

[40] K.K.W. Lo, J.S.Y. Lau,V.W.Y. Fong, Organometallic, 23 (2004) 1098.

[41] D. Brent McQueen, K.S. Schanze, J. Am. Chem. Soc., 113 (1991), 7470.

[42] M.W. Louie, H.W. Liu, M.H.Ch. Lam, T.Ch. Lau , K.K.W. Lo, Organometallics, 28 (2009) 4297.

[43] T. Morimoto, M. Ito, K. Koike, T. Kojima, T. Ozeki, O. Ishitani, Chem. Eur. J., 18 (2012) 3292.

[44] C. Bruckmeier, M.W. Lehenmeier, R. Reithmeier, B. Rieger, J. Herranz, C. Kavakli, Dalton Transactions, 41, (2012), 5026.

[45] S.A. Moya, J. Guerrero, R. Pastene, R. Schmidt, R. Sariego, R. Sartori, J. Sanz-Aparicio, I. Fonseca, M. Martinex-Ripoll, Inorg. Chem, 33 (1994) 2341.

[46] R. Czerwieniec, A. Kapturkiewicz, J. Lipkowski, J. Nowacki, Inorganica Chimica Acta, 358 (2005) 2701.

[47] P. Pyykko, Chem. Rev., 88 (1988) 563.

[48] B. Machura, M. Wolff, I. Gryca, A. Palion, K. Michalik, Polyhedron, 30 (2011) 2275.

[49] W.A. Rabanal-León; J.A. Murillo-López, D. Paez-Hernández, R. Arratia-Perez, J. Phys. Chem. A, 118 (2014) 11083.

[50] D. B. MacQueen, K.S. Schanze, J. Am. Chem.Soc, 113 (1991), 7470

[51] T. Liu, B.H. Xia, X. Zhou, H.X. Zhang, Q.J. Pan, J.S. Gao, Organometallics, 26 (2007) 143.

[52] R. Zhao, F.L. Wang, G. Liu, X. Shen, X. Wang, T. Yang, Z. Qiu, Y.J. Zhang, S. Jing, Y. Xu, D.R. Zhu, Inorganica Chimica Acta, 409 (2014) 372.